Super long green persistent luminescence from X-ray excited β-NaYF$_4$: Tb^{3+}

Yue Hu,[1] Yanmin Yang[1,*], Xiaoxiao Li,[1] Xin Wang,[1] Yunqian Li,[1] Tianyi Li,[1] Hongwu Zhang[2,*]

[1] College of Physics Science and Technology, Hebei University, Midwest universities comprehensive strength promotion project, Hebei Key Lab of Optic-electronic Information and Materials, Baoding, 071002, China.

[2] Institute of Urban Environment, Chinese Academy of Sciences, Xiamen 361021, China.

hwzhang@iue.ac.cn (Hongwu Zhang).

Abstract: Here, we have discovered a X-ray excited long afterglow phosphor β-NaYF$_4$: Tb^{3+}. After the irradiation of X-ray, the green emission can persist for more than 240 h. After 36 h, the afterglow intensity arrived at 0.69 mcd•m^{-2}, which can clearly be observed by naked eyes. Even after 84 h, the afterglow emission brightness still reached 0.087 mcd•m^{-2}. Also, combined with the results of thermoluminescence and photoluminescence, the super long afterglow emission of β-NaYF$_4$: Tb^{3+} can be ascribed to the tunneling model associated with *F* centers. More importantly, the super long green afterglow emission of β-NaYF$_4$: Tb^{3+} has been successfully used as *in vivo* light source to activate g-C$_3$N$_4$ for photodynamic therapy（PDT）and bacteria destruction. Furthermore, super long persistent luminescence of β-NaYF$_4$: Tb^{3+} could be repeatedly charged by X-ray for many circulations, which indicates that the phosphors have high photo stability under repeated cycles of alternating X-ray irradiation.

Keywords: long afterglow; tunneling model; *F* centers; PDT

In recent years, photodynamic therapy (PDT) has been believed as a novel antibiotic therapy in treating certain kinds of bacterial infections [1, 2]. Under an external light source, photosensitizers could be excited to induce cytotoxic reactive oxygen species (ROS) which exhibits broad spectrum antimicrobial activity and pathogenic bacteria do not readily develop resistance [3-9]. Usually, light sources used in PDT are mostly shortwave lasers, light emitting diodes (LEDs), and in some cases, arc lamps [10-14]. However, it is difficult to conduct antiseptic treatment in deep tissue due to the short penetration depth of light in tissues, which have limited the further application of PDT as novel antibiotics. It is well known that X-ray can penetrate much deeper through soft tissues than NIR light. Using X-ray as the irradiation source, a PDT process can be initiated in deep tissues (X-PDT). The theory was first proposed by Chen et al. [15] and the feasibility was demonstrated gradually with ZnS: Ag, CeF_3, CdSe [16, 17], those made of Y_2O_3 [18], GdO_2S: Tb [19], LaF_3: Ce [20], ZnO [21], SiC/SiO_x [22], TiO_2: Ce [23] and such [24-27]. However, X-ray could cause additional lesions on normal tissues and the scintillation nanoparticles need a large amount of X-ray irradiation and long irradiation time [28], which consequently increases the damage to human body. How to decrease the X-ray radiation dose is important for the development of PDT antibiotics.

Recently, long persistent luminescence phosphors (PLNPs) have attracted many attentions due to their wide application in bioimaging [29-32]. PLNPs can store the energy after Mercury or Xenon lamp exposure and then release luminescence slowly for several hours and even days without any excitation source [33]. In fact, these afterglow materials can also produce afterglow under X-ray excitation. Furthermore, the afterglow emission of X-ray excited long persistent luminescence phosphors (X-PLNPs) can be easily re-excited by the *in vivo* continuous X-ray excitation. In this way, the long term afterglow light can be used as *in vivo* exposure light to conduct PDT, which not only realize long time antiseptic treatment but also avoid the harm of X-ray radiation to health [34]. Up to now, several X-PLNPs, such as $ZnGa_2O_4$: Cr [35], $SrAl_2O_4$: Eu^{2+} [36], Yb^{3+} doped Gd－oxycarbonate [37] have been developed as bioimaging agents to realize long time *in vivo* imaging. At the same time, Ma group pioneered in demonstrating that

X-ray activated ZnS: Cu, Co afterglow nanoparticles－TBrRh123 conjugates for cancer cell destruction in vitro [38]. Chen and coworkers exploited $LiGa_5O_8$: Cr X-ray excited afterglow nanoparticles for imaging-guided X-ray induced photodynamic therapy of deep-seated tumors [39]. However, The usual afterglow material is charged by mercury lamp, and the excitation light is absorbed by valence electrons. When X-ray charging is used, the X-ray absorption is from the inner layer electron. Due to the different energy storage mechanism of the two afterglow materials, the better afterglow materials excited by mercury lamps are usually not ideal after X-ray excitation, which results in that the intensity of the developed X-PLNPs decayed quickly and is not strong enough to stimulate the photosensitizer. This meant that these phosphors cannot be regarded as efficient *in vivo* exposure light source to realize PDT. Furthermore, until now, as a novel afterglow phenomenon, the mechanism of X-ray excited long persistent luminescence is still unclear, which have limited the further development of novel higher efficiency X-PLNPs. Thus, exploring their luminescent mechanism and then development of novel higher efficiency X-PLNPs are indispensable to the design of PDT antibiotics in deep tissue.

In present work, we have successfully fabricated X-ray excited super long time green phosphors β-$NaYF_4$: Tb^{3+}, which not only can be quickly charged by X-ray and then emit green luminescence for several weeks after the removal of X-ray source but also can be excited by 980 nm laser to release the remaining energy efficiently. And, β-$NaYF_4$: Tb^{3+} is regarded as excellent model to explore the mechanism of X-ray excited long persistent luminescence in detail. Furthermore, since, g-C_3N_4, an excellent photocatalyst, possesses maximum absorption that overlaps with the emission of β-$NaYF_4$, X-ray excited long afterglow green light of β-$NaYF_4$: Tb^{3+} can be used as *in vivo* light source to activate g-C_3N_4 for PDT activation to inactivate bacteria Pseudomonas aeruginosa (PAO1). All the results have indicated that β-$NaYF_4$: Tb^{3+} possesses great potential as *in vivo* light source to realize PDT due to its X-ray excited super long afterglow properties.

Results

The XRD patterns and the electron micrographs of the as-prepared samples were shown in **Fig. 1a-b**. All the diffraction peaks of the samples were in perfect match with the standard powder peak positions of β-NaYF$_4$: Tb^{3+} hexagonal phase (JCPDF No. 16-0334) and no other phase and apparent shift can be found, indicating the as-prepared samples were pure β-NaYF$_4$. The TEM images showed that the samples consisted of uniform micro-rods with a diameter of ∼1 um. And, the hexagonal prisms morphology was further confirmed that the as-prepare samples were hexagonal β-NaYF$_4$. The X-ray excited emission spectrum (black) showed typical narrow emission peaks of Tb^{3+} which all show the A-band emission at 543 nm, as well as additional emission bands at 350-500 nm and 570-630 nm. All these peaks can be ascribed to the multiples transitions from f^8 [^{5}D$_3$] and 4f^8 [^{5}D$_4$] states to the lower energy ^{7}F$_J$ (**Supplementary Fig. 1**). The more important was that the sample possessed excellent X-ray induced afterglow properties, which afterglow emissions (red line, **Fig. 1c**) were similar to the photoluminescence and also can be ascribed to the transitions of Tb^{3+}. At the same time, we can observed the strong green afterglow emission from the Hebei University logo covered by the phosphors after irradiating by X-ray irradiation for 10 min in **Fig. 1d**, indicating the strong afterglow emission of β-NaYF$_4$: Tb^{3+}.

In order to further investigate the X-ray induced long persistence luminescent properties of β-NaYF$_4$: Tb^{3+}, the super long persistent luminescence decay curve of the ceramic discs monitored at 543 nm after irradiation by an X-ray irradiator for 10 min had been obtained as shown in **Fig. 2a**. The afterglow intensity decreased quickly in the first several hours and then decays slowly. Even after 36 h, the afterglow intensity still arrived at 0.69 mcd•m^{-2}, which can be can be clearly observed by naked eyes. Even after 84 h, the afterglow emission brightness still reached 0.087 mcd•m^{-2} (**Fig. 2c**). In addition, the inset of **Fig. 2a** gave afterglow spectra acquired at different times during the 20 days afterglow process.

4

The profiles of the afterglow spectra did not change with decay time, indicating that the persistent luminescence originated from the Tb^{3+} emitting centres and existed in the whole photoluminescence emission band. Even compared with background, the afterglow spectrum of β-NaYF$_4$: Tb^{3+} can be clearly measured after 20 days. The long-lasting afterglow of the phosphors was further confirmed by a digital SLR camera. **Fig. 2b** showed the change in afterglow brightness over time for four discs after exposure to a 30 mA 50 KV X-ray irradiator for different time. The green afterglow light can be rapidly charged and even 1 min X-ray irradiation can induce more than ten days of persistent visible emission. At the same time, the enhancement of X-ray irradiation time can obviously prolong the afterglow time and increase the afterglow intensity. Among the 10-15 min irradiation was the most suitable for X-ray induced long persistence luminescence of β-NaYF$_4$: Tb^{3+}, which was consistent with the afterglow curves induced different irradiation time (**Supplementary Fig. 2**), considering the reduction of X-ray dosage makes sense here we chose X-ray irradiation for 10 min. Furthermore, when the afterglow emissions decayed undetectable after 240 h, the 100℃ heat-treatment can induce the recovery of the strong green emission (**Fig. 2b-7**) which became even brighter than the ones that underwent 5 min of decay (**Fig. 2b-1**). This can be ascribed to the rapid and massive release of the residual trapped electrons located in traps by the heat. More important, this intensive release process lasted for more than 10 min until the traps are completely emptied. The heat-assisted intense visible emission indicates that the energy released during the 240 h RT decay process was just part of the energy collected and stored by the materials during excitation and thus that the actual decay time should be much longer than 240 h. All these results have indicated that β-NaYF$_4$: Tb^{3+} possessed super-long green afterglow emission under the irradiation of X-ray.

Due to its X-ray-excited super long green persistent luminescence, β-NaYF$_4$: Tb^{3+} can be potentially regarded as *in vivo* light source to activate photosensitizer to conduct PDT in deep tissue. Owing to strong absorption of blue-green light, g-C$_3$N$_4$ (**Supplementary Fig. 3**), a famous photo-

catalyst, was chosen as PDT agent combined with β-NaYF$_4$: Tb^{3+} to treat bacterial infection in deep implant. It is well known that PAO1 is a common gram-negative rod-shaped bacterium that is susceptible to cause diseases in organisms [40] and used here as processing object (**Supplementary Fig. 4** and **Fig. 5**). Experimental data indicated that after irradiated for 2 min by X-ray under 30 mA 50 kVp, treated with the composite of β-NaYF$_4$: Tb^{3+}- g-C$_3$N$_4$, the viabilities of PAO1 cells rapidly decreased to 67.14%, while the X-ray irradiation hardly induced the harm to the growth of PAO1 in the control group (**Fig. 5a**). More importantly, it could be observed that after remove of X-ray source, during 5 h, the viabilities of PAO1 cells could decrease largely to about 30.92% (**Fig. 5f** and **Fig. 5g**), which indicated that the X-ray excited afterglow emission of β-NaYF$_4$: Tb^{3+} could continuously provide light energy to activate g-C$_3$N$_4$, which thus largely prolonged the photodynamic treating time and obviously decrease the X-ray irradiation dose. These results suggest that X-ray excited long afterglow green emission of β-NaYF$_4$: Tb^{3+} would develop a novel PDT method with more safety and efficient for future medical therapy.

Discussion

It is well known that thermally stimulated luminescence (TSL) can only explore shallow traps due to the high temperature can cause the thermal quenching of the luminescent center and photo stimulated luminescence (PSL) can explore deeper traps [41-45]. Thus, here, the TSL and PSL methods were utilized to explore the mechanism of X-ray induced super long afterglow emission of β-NaYF$_4$: Tb^{3+}. No TSL spectrum from the sample was detected after being excited by UV lamp, however, a strong TSL emission at 107℃ occurs from the 4f^8 → 7f$_J$ transition of Tb^{3+} after X-ray excitation as shown in **Fig. 3a**. Since β-NaYF$_4$: Tb^{3+} was a broad bandgap material (7.3 eV), UV light was not enough sufficient to charge defects but the X-ray irradiation can provide high energy to realize the charge of traps. **Supplementary Fig. 6** showed a clear linear relationship between the reciprocal of the square of the

persistent luminescence intensity (I^{-1}) at 543 nm and time (t) in the latter stage of the decay of the afterglow which confirmed that a tunneling process occurs [46-48]. The persistent luminescence at -196°C more confirmed the tunneling process (**Supplementary Fig. 7**). Then the trap depth was estimated to be 0.764 eV via the equation of $E=2kT_m^2/\delta_T$ [49]. In order to explore the nature of the deeper traps, we further stimulated the sample locally by 450 nm, 532 nm, 635 nm, 808 nm and 980 nm fiber lasers respectively after X-ray charging. The afterglow intensity of the laser-irradiated portion was enhanced after a short period of irradiation, and as the irradiation time increased, the afterglow fluorescence rapidly weakened and eventually disappeared completely (**Fig. 3b**). The part that was blackened by laser irradiation will not show the afterglow emission even if it was heated (**Supplementary Video 1**). However, if the shallow trap electrons were completely released by high-temperature heating before the laser irradiation, the afterglow illumination can be seen again in the portion excited by the laser after the short time irradiation was stopped (**Supplementary Video 2**). All of these phenomena lead us to believe that under laser excitation, part of the electrons of the deep traps will be transferred to the shallow traps, and the other part will act to illuminate with the center of the luminescence. In a short time, the former was dominant and the afterglow emission was enhanced; when the excitation time was increased, the latter was dominant and the afterglow emission was weakened.

The color center phenomena of halide alkali metal was studied in depth in the 1920s and 1970s, which provided a theoretical basis for the fluoride afterglow mechanism [50-54]. Hence, we proposed a tunneling model associated with F centers (**Fig. 4a**). The simple process of storing and releasing energy is: the electrons of VB (electrons in F 2p orbital) are excited to the CB (free state) after the sample is excited via X-ray, they will drop to the bottom of the CB (Y 4d orbital) after loss of kinetic energy (**Fig. 4a①** and **Fig. 4b ⅰ**). Meanwhile, portion of the F^- ions are excited by X-ray to escape, resulting in F vacancies, while the electrons at the bottom of the CB will be captured by F-vacancies to form F-centers

(the electron of Y 4d orbital shifts into F vacancies (**Fig. 4a②** and **Fig. 4b ⅲ**)). Tb^{3+} ion is easy to lose an electron to a stable structure with eight electrons in its outermost shell (equivalent to capturing a hole from the VB and the electron will fill the F 2p orbital (**Fig. 4a③** and **Fig. 4b ⅱ**)) to form Tb^{4+} [55, 56]. At this point, the F center forms tight bound exciton (Frenker exciton) with Tb^{4+} ion [57, 58], the electron in F center and the hole bound by Tb^{3+} are directly recombined through tunneling process (**Fig. 4c3** and **Fig. 4b ⅳ**), the ground state electron of Tb^{3+} absorb energy and are activated to a high energy state and then followed by luminescence of the 4f $\rightarrow$ 4f transition.

Although the recharge and release process from above can explain the afterglow phenomenon, it cannot explain the extra long afterglow properties of this material. Based on the light excitation and thermal excitation data, we realize that there are deep traps and shallow traps, and electrons can pass between them. In fact, R. W. Pohl has already studied the electron transfer between deep traps and shallow traps in fluoride, and pointed out that the deep trap is F centers , and the shallow trap is from F' centers [50]. Hence, the simple electron transfer process of F centers and F' centers with tunneling process was shown in **Fig. 4c**. The electron in the F center nearest of the luminescent center is easily recombined with the luminescent center through Auger effect to leave the F vacancy (**Fig. 4c1**). The electron of the F' center enter the F vacancy through tunneling energy level under thermal excitation to form a new F center (**Fig. 4c2**) and then recombine with the luminescence center through Auger effect (**Fig. 4c3**). The energy required for this process is low, which is the initial process of afterglow decay at RT. The electron in F center recombine with the F vacancy adjacent to the luminescent center through tunneling effect to form a new F center to achieve the energy transfer between the F centers (**Fig. 4c5**), and causing the luminescent center to recombine with its nearest neighbor F center (**Fig. 4c6**). The energy required for this process is high, which is the slow decay process of the afterglow at RT. Although the above model can explain the long afterglow phenomenon, the actual situation is much more complicated.

The color center includes not only F centers, but also R centers, M centers, etc [52]. How they interact with each other requires more research.

In summary, We have developed β-NaYF$_4$: Tb^{3+} persistent phosphors that can be effectively activated by X-ray and exhibit super long lasting visible afterglow. After the irradiation of X-ray, the green emission can persist for more than 240 h. After 36 h, the afterglow intensity arrived at 0.69 mcd•m^{-2}, which can clearly be observed by naked eyes. Even after 84 h, the afterglow emission brightness still reached 0.087 mcd•m^{-2}. Furthermore, due to the excellent overlap between the afterglow emissions of β-NaYF$_4$: Tb^{3+} and the absorption of g-C$_3$N$_4$, β-NaYF$_4$: Tb^{3+} has been explored as irradiation source to activate the g-C$_3$N$_4$ to conduct PDT. The obtained results showed that the afterglow emission of β-NaYF$_4$: Tb^{3+} can inhibit the viabilities of PAO1 cells largely to about 30.92% during 5 h after ceasing the X-ray irradiation. Furthermore, super long green light of β-NaYF$_4$: Tb^{3+} could be repeatedly charged by a X-ray activation for many circulations, which indicated that the phosphors had high photo stability under repeated cycles of alternating X-ray irradiation. All the results suggested that X-ray excited long afterglow green emission of β-NaYF$_4$: Tb^{3+} would develop a novel PDT method with more safety and efficient for future medical therapy.

Materials and methods

Synthesis of β-NaYF$_4$: Tb^{3+} phosphors: The raw materials used for synthesis of β-NaYF$_4$: Tb^{3+} phosphors were Tb(NO$_3$)$_3$•6H$_2$O (of 99.99% purity) and Y(NO$_3$)$_3$·6H$_2$O (of 99.99% purity) (all from Aladdin Industrial Inc. Shanghai, China), NaNO$_3$ (of 99.95% purity), NH$_4$F (of 99.9% purity), EDTA-2Na (of 99.9% purity) and HNO$_3$ were purchased from Sinopharm Chemical Reagent Co.Ltd. (Shanghai, China).

β-NaYF$_4$: 10%Tb^{3+} (**Supplementary Fig. 8**) microparticles (MPs) were produced through a conventional Hydrothermal method, Briefly, according to the designed composition certain amount of

$NaNO_3$, $Y(NO_3)\cdot 6H_2O$ and $Tb(NO_3)_3\cdot 6H_2O$ were weighed and dissloved in deionized water with a molar ratio of 1.0:0.9:0.1. An aqueous solution containing EDTA-2Na (5 mmol) was then added to the above solution and stirred slowly for 30 min. Also 40 mmol of NH_4F were dissolved in the deionized water Using ultrasound and added into the mixture and then adjusted the PH to 5 with dropping dilute HNO_3. After vigorous stirring for another 30 min, The final mixture was transferred into a stainless Teflon-lined autoclave, sealed and maintained at 180°C for 20 h. As the system was spontaneously cooled to room temperature, the reaction products were collected by centrifugation and washed in ethanol for three times, then dried at 80°C for 24 h, finally ground to obtain fine β-$NaYF_4$: 10%Tb^{3+} phosphors.

The obtained powder (3 g) was pressed into discshaped samples respectively with diameters of 10 mm using a uniaxial hydraulic press at a pressure of 15 MPa.

Synthetic of g-C₃N₄: The photocatalyst of g-C_3N_4 was prepared by directly heating melamine in the semiclosed system to prevent sublimation of melamine. 10 g of melamine powder was put into an alumina crucible with a cover, then heated to 500°C in a muffle furnace for 2 h at a heating rate of 20°C/min; the further deammonation treatment was performed at 520°C for 2 h.

Bacterial culture: All glass apparatuses used in the experiments were autoclaved at 121°C for 20 min to ensure sterility. pseudomonas (P.) aeruginosa PAO1 was grown in the beef extract peptone medium incubator at 35°C.Three days later, the sealing film on the culture dish with cultivate good bacteria was stripped, and the appropriate size quartz plate was fixed on the mouth of the Petri dish. The initial PAO1 population in this batch medium was about 106 colony-forming units (cfu)/mL.

Bacterial inactivation by X-PDT: Prior to each experiment, the discshaped samples were sterilized first by burning with alcohol lamp for about 2 min and fixed in a sterile petridish with a Whatman® No.2

filter paper at the bottom. The petri dishes containing sterilized coupons were then further sterilized under germicidal UV light (254 nm) for 30 min in a biosafety cabinet. Here a total of six groups of experiments were compared. The two batch mediums with initial PAO1 labeled as group1 and group2 respectively. The four batch mediums with initial PAO1 were incubated in the dark at RT for 30 min with 0.5 ml of g-C_3N_4 in PBS labeled as group3-6 respectively. For a more realistic expreimental scenario, an 1 cm thick pork skin tissue was fixed at the bottom of each medium. Group1 was irradiated from the bottom of the mediums by X-ray under 30 mA, 50 kVp for 2 min. Group2 with β-$NaYF_4$: Tb^{3+} phosphors covering at the top of the mediums was irradiated from the bottom of the mediums by X-ray which the irradiation time and the power density were the same as that of group1. Group3 was a blank control. Likewise, group4 performed the same steps as group1. Group5 repeated the procedure of group2 but took β-$NaYF_4$: Tb^{3+} phosphors away immediately after ceasing the X-ray irradiation. Group6 strictly repeated the procedure of group2. Then all groups were placed for five hours. All of the above experiments were conducted in dark environment in order to rule out any inactivation effect due to the other light.

Testing photodynamic sterilization property. The BacLight Live/Dead bacterial viability kit (L-7012; Molecular Probes) was used to evaluate cell membrane integrity. The kit contains Syto9 and propidium iodide to differentiate between cells with intact membranes (live) and membrane-damaged cells (dead), respectively. The stain was prepared by dilution of 3 μL of each component into 1mL of distilled water, and placed in the dark for 15 min. When these preparations were analyzed, at least 2000 cells were scored per sample. 1 μL of the mixed solution was dropped onto a glass slide and was photoirradiated under onfocal laser scanning microscope observation. A water immersion objective lens was used. The optimum photomultiplier setting was determined in a pre-experiment, and then the same photomultiplier setting was used for all the samples.

11

Characterization. The structural characterization of the synthesized phosphors were supported by X-ray diffraction (XRD) with Bruker D8 advance X-ray diffractometer (Bruker Optics, Ettlingen, Germany) using CuKα radiation at a scanning step of 0.02°. The morphology of the prepared samples was obtained using a Nova Nano SEM200 scanning electron microscope (FEI, Inc.). X-ray excited emission spectra, afterglow emission spectra and afterglow decay curves were recorded using an Andor SR-500i spectrometer (Andor Technology Co. Belfast, UK) equipped with a Hamamatsu R928 photomultiplier. The thermoluminescence (TSL) spectra of samples were measured using a FJ-427A1TL dosimeter (Beijing Nuclear Instrument Factory, China) with a fixed heating rate of 1 K/s within the range 350-550 K. The afterglow phosphors were excited using an XRad-320 X-ray irradiator (Precision X-ray, Inc., North Branford, CT) under 30 mA, 50 kVp, the trapping states (trap depth and type) were measured using 450 nm, 488 nm, 532 nm, 808 nm and 980 nm fiber lasers with collimating lens respectively, and the afterglow images were recorded using a digital SLR camera (EOS 5D Mark III) via a PVS-14 Generation III night vision monocular in a dark room. The brightness attenuation is measured by a gentec pronto laser power meter (Pronto Si, Gentec-EO, Canada). The micrographs of biofilms on culture dishes were imaged with a laser scanning confocal microscope (Olympus, Fv1000, Germany).

References

1.   Barra F, Roscetto E, Soriano A A, et al. Photodynamic and Antibiotic Therapy in Combination to Fight Biofilms and Resistant Surface Bacterial Infections. *Int. J. Mol. Sci*. **16,** 20417-20430 (2015).

2.   Macdonald I J, Dougherty T J. Basic principles of photodynamic therapy. *J. Porphyrins Phthalocyanines*. **5,** 105-129 (2001).

3. Macdonald I J, Dougherty T J. Basic principles of photodynamic therapy. *J. Porphyrins. Phthalocyanines.* **5,** 105-129 (2001).

4. Fakharealam M, Kishwar S, Siddique M, et al. The Photodynamic effect of ZnO nanorods and their ligands with different photosensitizers. *J. Nanosci. Nanotechno.* **1,** 40-51 (2012).

5. Strassert C A, Otter M, Albuquerque R Q, et al. Photoactive hybrid nanomaterial for targeting, labeling, and killing antibiotic-resistant bacteria. *Angew. Chem. Int. Edit.* **48,** 7928-7931 (2009).

6. Zhao, Zhiwei, et al. A bacteria-activated photodynamic nanosystem based on polyelectrolyte-coated silica nanoparticles. *J. Mater. Chem B.* **5,** 3572-3579 (2017).

7. Hashimoto M C, Prates R A, Kato I T, et al. Antimicrobial photodynamic therapy on drug-resistant Pseudomonas aeruginosa-induced infection. An *in vivo* study. *Photochem. Photobiol.* **88,** 590-595 (2012).

8. Jijie R, Dumych T, Li C, et al. Particle-based photodynamic therapy based on Indocyanine green modified plasmonic nanostructures for inactivation of Crohn's disease‐associated Escherichia coli. *J. Mater. Chem B.* **4,** 2598-2605 (2016).

9. Li X, Lee S, Yoon J. Supramolecular photosensitizers rejuvenate photodynamic therapy. *Chem. Soc. Rev.* **47,** (2018).

10. Allison R R, Mang T S, Wilson B D. Photodynamic therapy for the treatment of nonmelanomatous cutaneous malignancies. *Semin. Cutan. Med. Surg.* **17,** 153-163 (1998).

11. Wang S, Gao R, Zhou F, et al. Nanomaterials and single oxygen photosensitizers: Potential applications in photodynamic therapy. *J. Mater. Chem.* **14,** 487-493 (2004).

12. Chen H, Wang G D, Chuang Y J, et al. Nanoscintillator-mediated X-ray inducible photodynamic therapy for *in vivo* cancer treatment. *Nano Lett*. **15,** 2249-2256 (2015).

13. Wang C, Cheng L, Liu Z. Upconversion Nanoparticles for Photodynamic Therapy and Other Cancer Therapeutics. *Theranostics*. **3,** 317-330 (2013).

14. Wilson B C. Photodynamic therapy for cancer: principles. *Can. J. Gastroenterol*. **16,** 393-396 (2002).

15. W. Chen and J. Zhang, Using nanoparticles to enable simultaneous radiation and photodynamic therapies for cancer treatment, *J. Nanosci. Nanotechnol*. **6,** 1159-1166 (2006).

16. Takahashi J , Misawa M . Analysis of Potential Radiosensitizing Materials for X-Ray-Induced Photodynamic Therapy. *Nanobiotechnology*. **3,** 116-126 (2007).

17. Clement S, Deng W, Camilleri E, et al. X-ray induced singlet oxygen generation by nanoparticle-photosensitizer conjugates for photodynamic therapy: determination of singlet oxygen quantum yield. *Sci. Rep.* **6,** 19954 (2016).

18. J. P. Scaffidi,M. K. Gregas, B. Lauly, Y. Zhang and T. Vo-Dinh, Activity of Psoralen-Functionalized Nanoscintillators against Cancer Cells upon X-ray Excitation. *ACS Nano.* **5,** 4679-4687 (2011).

19. Abliz E, Collins J E, Bell H, et al. Novel applications of diagnostic X-rays in activating a clinical photodynamic drug: Photofrin II through X-ray induced visible luminescence from" rare-earth" formulated particles. *J. X-ray Sci. Technol.* **19,** 521-530 (2011).

20. Zou X, Yao M, Ma L, et al. X-ray-induced nanoparticle-based photodynamic therapy of cancer. *Nanomedicine*. **9,** 2339-2351 (2014).

21.   Generalov R, Kuan W B, Chen W, et al. Radiosensitizing effect of zinc oxide and silica nanocomposites on cancer cells. *Colloid. Surface B*. **129,** 79-86 (2015).

22.   Rossi F, Bedogni E, Bigi F, et al. Porphyrin conjugated SiC/SiO x nanowires for X-ray-excited photodynamic therapy. *Sci. Rep*. **5,** 7606 (2015).

23.   Yang C C, Sun Y J, Chung P H, et al. Development of Ce-doped TiO2 activated by X-ray irradiation for alternative cancer treatment. *Ceram. Int*. **43,** 12675-12683 (2017).

24.   S. Kascakova, A. Giuliani, S. Lacerda, A. Pallier, P. Mercere, E. Toth and M. Refregiers, X-ray-induced radiophotodynamic therapy (RPDT) using lanthanide micelles: Beyond depth limitations. *Nano Res*. **8,** 2373－2379 (2015).

25.   Homayoni H, Jiang K, Zou X, et al. Enhancement of protoporphyrin IX performance in aqueous solutions for photodynamic therapy. *Photodiagn. Photodyn*. **12,** 258-266 (2015).

26.   Y. G. Tang, J. Hu, A. H. Elmenoufy and X. L. Yang, Highly Efficient FRET System Capable of Deep Photodynamic Therapy Established on X-ray Excited Mesoporous LaF$_3$: Tb Scintillating Nanoparticles. *ACS Appl. Mater. Inter*. **7,** 12261-12269 (2015).

27.   Chen H, Wang G D, Chuang Y J, et al. Nanoscintillator-mediated X-ray inducible photodynamic therapy for *in vivo* cancer treatment. *Nano Lett.* **15,** 2249-2256 (2015).

28.   Liu Y, Chen W, Wang S, et al. Investigation of water-soluble x-ray luminescence nanoparticles for photodynamic activation. *Appl. Phys. Lett*. **92,** 043901-043901-3 (2008).

29.   Maldiney, T. *et al.* The *in vivo* activation of persistent nanophosphors for optical imaging of vascularization, tumours and grafted cells. *Nat. Mater.* **13,** 418-426 (2014).

30.   Xue Z, Li X, Li Y, et al. X-ray-activated near-infrared persistent luminescent probe for deep-

        tissue and renewable *in vivo* bioimaging. *ACS Appl. Mater. Inter*. **9,** 22132-22142 (2017).

31.   Li J L, Shi J P, Wang C C, et al. Five-nanometer $ZnSn_2O_4$: Cr, Eu ultra-small nanoparticles as

        new near infrared-emitting persistent luminescent nanoprobes for cellular and deep tissue

        imaging at 800 nm. Nanoscale, **9,** 8631-8638 (2017).

32.   Maldiney, T. *et al.* Controlling electron trap depth to enhance optical properties of persistent

        luminescence nanoparticles for *in vivo* imaging. *J. Am. Chem. Soc.* **133,** 11810-11815 (2011).

33.   Pan, Z., Lu, Y. Y., Liu, F. Sunlight-activated long-persistent luminescence in the near-infrared

        from Cr^{3+}-doped zinc gallogermanates. *Nat. Mater.* **11,** 58-63 (2011).

34.   Chen W. Nanoparticle Self-Lighting Photodynamic Therapy For Cancer Treatment. *J. Biomed.

        Nanotechnol*. **4,** 369-376 (2008).

35.   Xue Z , Li X , Li Y , et al. X-ray Activated Near-infrared Persistent Luminescent Probe for Deep-

        tissue and Renewable *In Vivo* Bioimaging. *ACS Appl. Mater*. *Inter*. **9,** (2017).

36.   Song L, Lin X H, Song X R, et al. Repeatable deep-tissue activation of persistent luminescent

        nanoparticles by soft X-ray for high sensitivity long-term *in vivo* bioimaging. *Nanoscale.* **9,** 2718

        (2017).

37.   Caratto V , Locardi F , Costa G A , et al. NIR Persistent Luminescence of Lanthanide Ion-Doped

        Rare-Earth Oxycarbonates: The Effect of Dopants. *ACS Appl. Mater*. *Inter.* **6,** 17346-17351

        (2014).

38.   Ma L, Zou X, Bui B, et al. X-ray excited ZnS:Cu,Co afterglow nanoparticles for photodynamic

        activation. *Appl. Phys. Lett*. **105,** 105 (2014).

39.   Chen H, Sun X, Wang G D, et al. LiGa$_5$O$_8$: Cr-based theranostic nanoparticles for imaging-guided X-ray induced photodynamic therapy of deep-seated tumors. *Mater. Horiz.* **4,** 1092-1101 (2017).

40.   Johnson, T. A., Rehak, E. A., Sahu, S. P., Ladner, D. A., Cates, E. L. Bacteria Inactivation via X-ray-Induced UVC Radioluminescence: Toward in Situ Biofouling Prevention in Membrane Modules. *Environ. Sci. Technol.* **50,** 11912-11921 (2016).

41.   Rodrigues L C V, Hölsä J, Lastusaari M, et al. Defect to R^{3+} Energy Transfer: Colour Tuning of Persistent Luminescence in CdSiO$_3$. *J. Mater. Chem. C.* **2,** 1612-1618 (2013).

42.   Li Y, Zhou S, Li Y, et al. Long persistent and photo-stimulated luminescence in Cr^{3+}-doped Zn-Ga-Sn-O phosphors for deep and reproducible tissue imaging. *J. Mater. Chem. C.* **2,** 2657-2663 (2014).

43.   Aitasalo, T., Hölsä, J., Jungner, H., Lastusaari, M., Niittykoski, J. Thermoluminescence Study of Persistent Luminescence Materials: Eu^{2+}- and R^{3+}-Doped Calcium Aluminates, CaAl$_2$O$_4$:Eu^{2+},R^{3+}. *J. Phys. Chem. B.* **110,** 4589-4598 (2006).

44.   Yamada M, Mizuguchi M, Nishimaki K, et al. Optical absorption and ESR study of F centres in BaClF and SrClF crystals. *J. Phys. Chem. Solids.* **37,** 961-966 (1976).

45.   Von Seggern H, Voigt T, Knupfer W, et al. Physical model of photostimulated luminescence of x-ray irradiated BaFBr: Eu^{2+}. *J. Appl. Phys.* **64,** 1405-1412 (1988).

46.   Avouris P, Morgan T N. A tunneling model for the decay of luminescence in inorganic phosphors: The case of Zn$_2$SiO$_4$: Mn. *J. Chem. Phys.* **74,** 4347-4355 (1981).

47.   Trojan Piegza, J., Niittykoski, J., Hölsä, J., Zych, E. Thermoluminescence and Kinetics of

       Persistent Luminescence of Vacuum-Sintered Tb^{3+}-Doped and Tb^{3+},Ca^{2+}-Codoped Lu_2O_3

       Materials. *Chem. Mater.* **20,** 2252-2261 (2008).

48.   Mendenhall G D, Agarwal H K. Slow luminescence emission from polymers with a hyperbolic

       decay law. A survey of commercial materials with an apparatus of wide aperture. *J. Appl. Polym.*

       Sci. **33,** 1259-1274 (1987).

49.   Bos A J J. High sensitivity thermoluminescence dosimetry. *Nucl. Instrum. Meth. B*. **184,** 3-28

       (2001).

50.   Pohl R W. Electron conductivity and photochemical processes in alkali-halide crystals. *Proc.*

       Phys. Soc. **49,** 3-31 (1937).

51.   Mott N F, Gurney R W. Electronic processes in ionic crystals. *OUP*. (1948).

52.   Seitz F. Color centers in alkali halide crystals. *Rev Mod Phys.* **18,** 384 (1946).

53.   Schulman J H, Compton W D. Color centers in solids. *Pergamon*. (1962).

54.   Garbuny B M. Optical physics. *Academic Press*. (1965).

55.   Dorenbos, P. Systematic behaviour in trivalent lanthanide charge transfer energies. *J. Phys:*

       Condens. Mat. **15,** 8417-8434 (2003).

56.   Dorenbos P, Bos A J J. Lanthanide level location and related thermoluminescence phenomena.

       Radiat. Meas. **43,** 139-145 (2008).

57.   Frenkel J. On the Transformation of light into Heat in Solids. *Phys. Rev*. **37,** 1276-1294 (1931).

58.   Schwentner N, Koch E E, Jortner J. Electronic Excitations in Condensed Rare Gases. *Springer-Verlag*. (1985).

Acknowledgement

Author contributions

The manuscript was written through contributions of all authors. All authors have given approval to the final version of the manuscript.

Additional information

Supplementary Information is linked to the online version of this paper at http://www.nature.com/.

Competing financial interests

The authors declare no competing financial interests.

Reprint and permissions information is available at http://www.nature.com/.

Figures

Figure 1. | **Structure, composition, and optical properties of raw β-NaYF₄: 10%Tb³⁺. a**, X-ray diffraction (XRD) pattern of β-NaYF₄, the position of XRD peaks of the β-NaYF₄ crystalline are shown at the below. **b**, The electron microscopy image of the synthesized phosphors recorded at high magnification corresponding to its phases. **c**, X-ray excited luminescence spectra (black) and afterglow spectra (red) of the phosphors. **d**, A paint of the Hebei University logo prepared by mixing raw phosphors with anhydrous ethanol. The logo is photographed after being irradiated by X-ray irradiation for 10 min. Strong green luminescence is emitted from the material. The paint is taken by a digital SLR camera. The imaging parameter is: auto/ISO 200/0.5 sec.
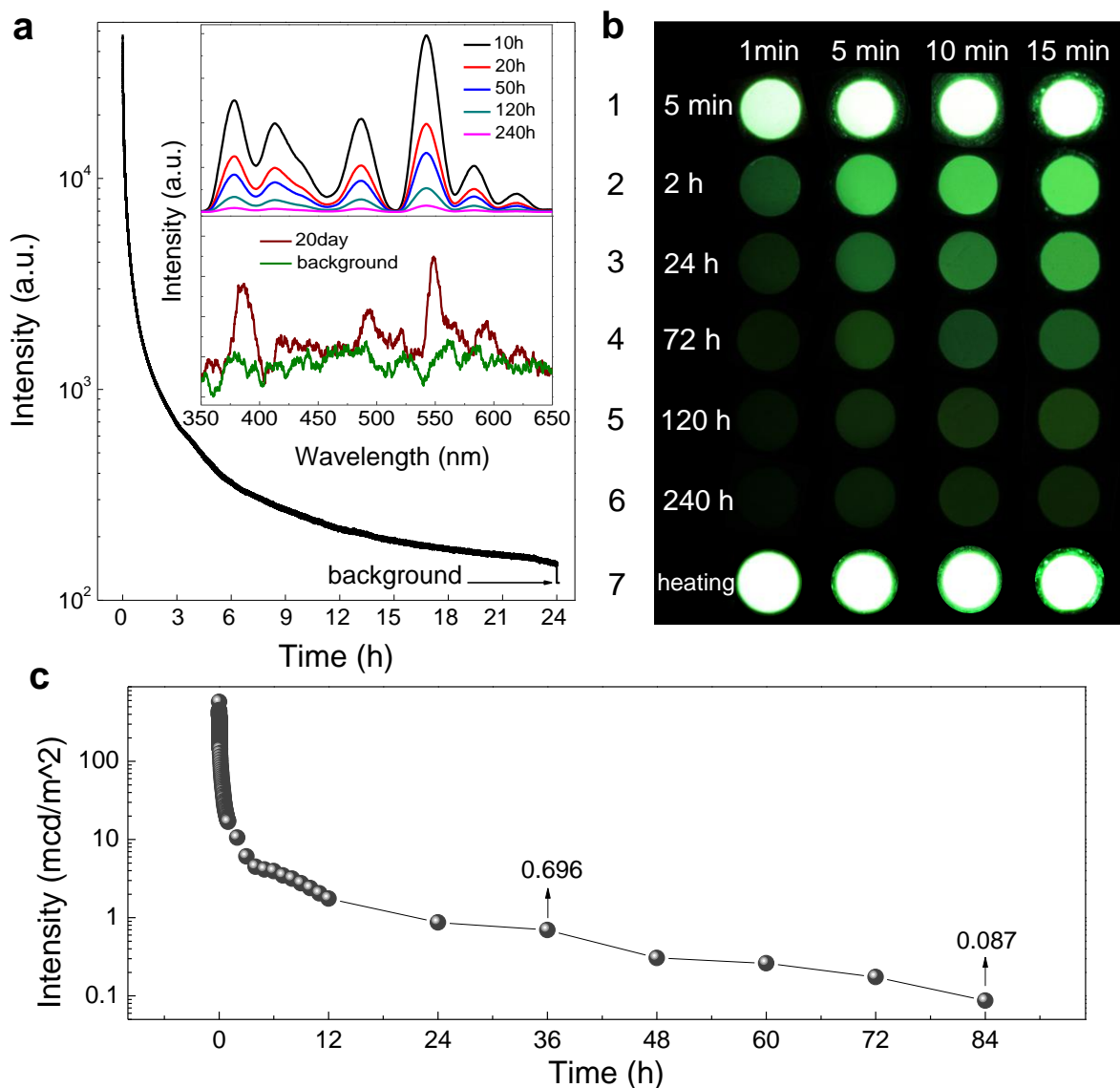
Figure 2. | long visible afterglow decay of the sample discs irradiated by a 30 mA 50 KV X-ray irradiator. a,

Afterglow intensity from β-NaYF$_4$: Tb^{3+} monitored at 543 nm as a function of time. The samples was irradiated for 10

min. The upper inset shows six afterglow spectra of the phosphors recorded at 10 h, 20 h, 50 h, 120 h, 240 h and 20 day

after the stoppage of the irradiation. **b-1–b-6**, images of four sample discs taken at different afterglow times (5 min to

240 h) after irradiation by X-ray for 1 min to 15 min. The discs were placed on a black plate surface for imaging in a

dark room. Imaging parameters: b-1, auto/ISO 200/0.3 s; b-2, manual/ISO 200/30 s; b-3, manual/ISO 400/1 min. b-4,

manual/ISO 400/2 min. b-5, manual/ISO 400/ 3 min. b-6, manual/ISO 400/ 4 min. **b-7**, image of the four 240 h-

decayed discs when heated at 100°C on the hot plate in a dark room. Imaging parameters: auto/ISO, 200/0.3 s. **c**,

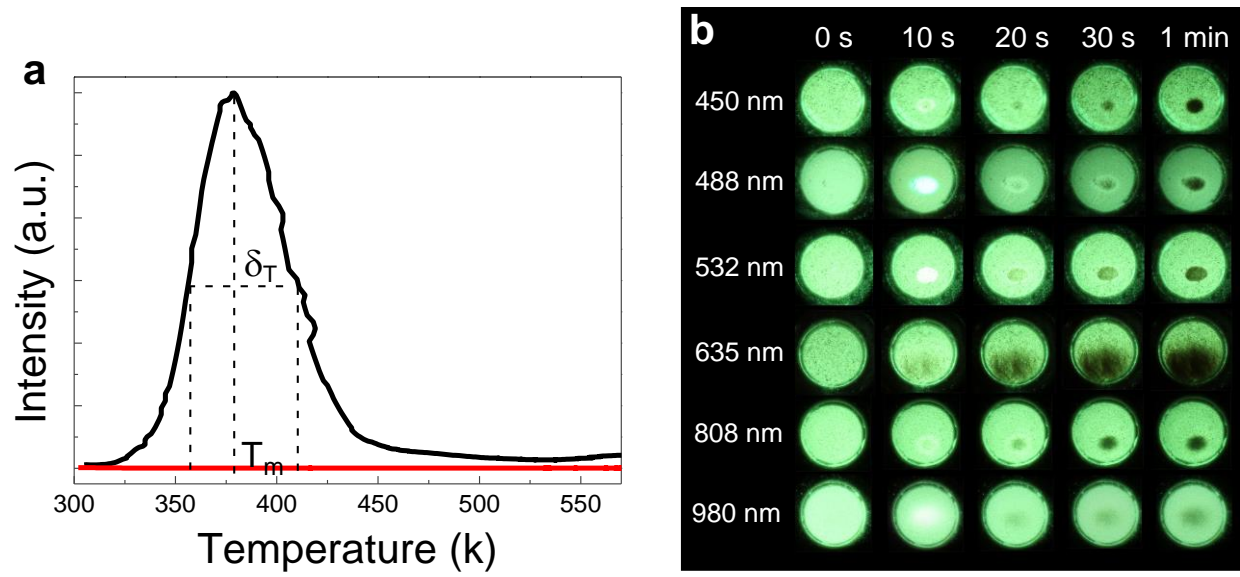Afterglow brightness of β-NaYF$_4$: Tb^{3+} as a function of time taken after 10 min X-ray excitation.

Figure 3. | TSL and PSL of β-NaYF₄: Tb³⁺. a, TSL curves of the phosphors are measured both after the stoppage of X-ray irradiation using a W source and UV lamp (254 nm) for 5 h respectively. **b**, Contrastive images of X-ray excited sample discs again partially stimulated by 450 nm, 488 nm, 532 nm, 635 nm, 808 nm and 980 nm fiber laser, respectively. Power: 0.081 W, 0.033 W, 0.025 W, 0.065 W, 1 W, 2 W, respectively.
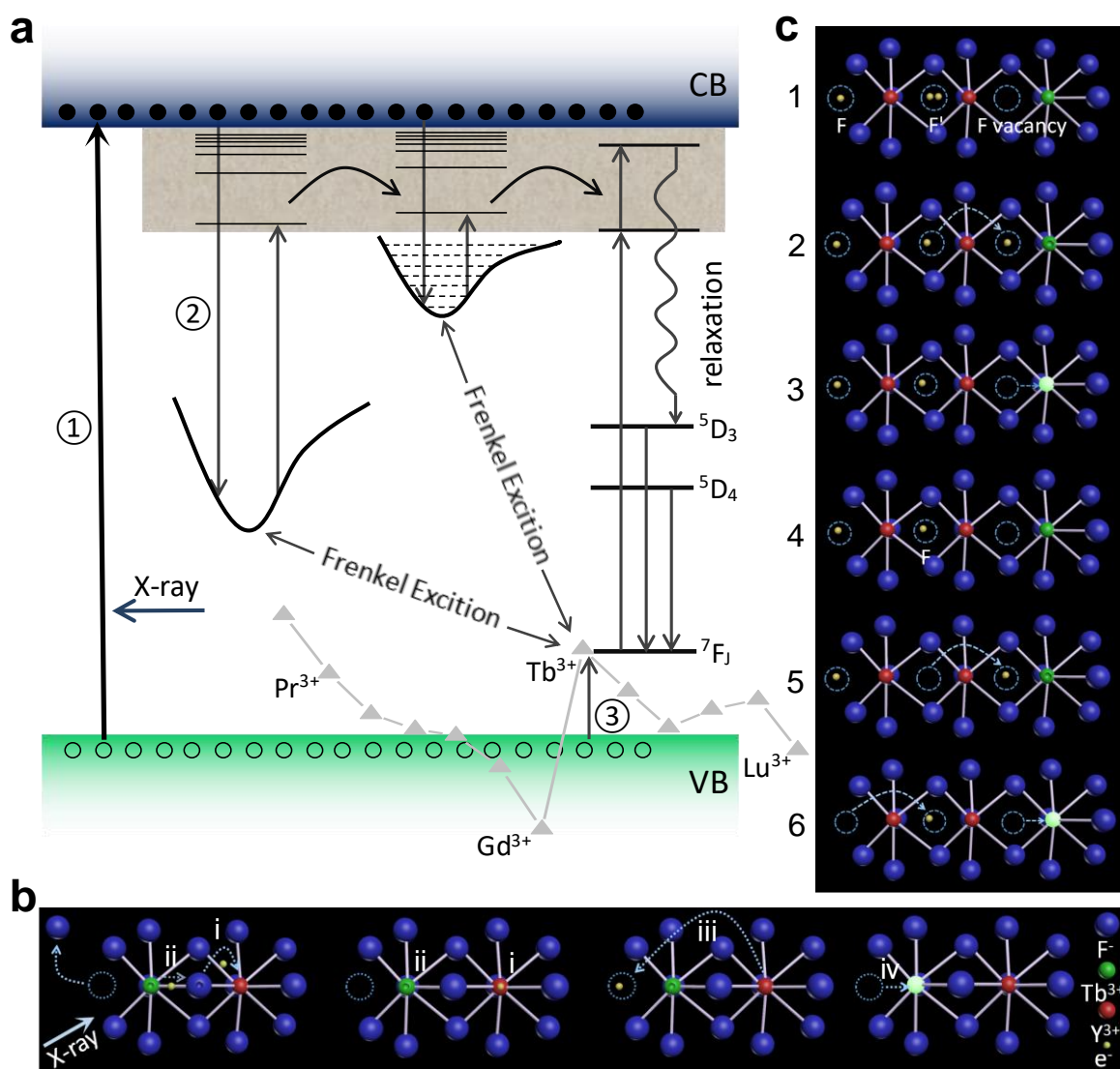
Figure 4. | Schematic illustration of afterglow mechanism. a, Spatial Schematic Diagram of multi-tunneling energy levels affected by F and F' center. **b**, Schematic representation of the X-ray excited persistent luminescence multi-tunneling energy levels model. **c**, Spatial Mechanism of X-ray excited Luminescence.
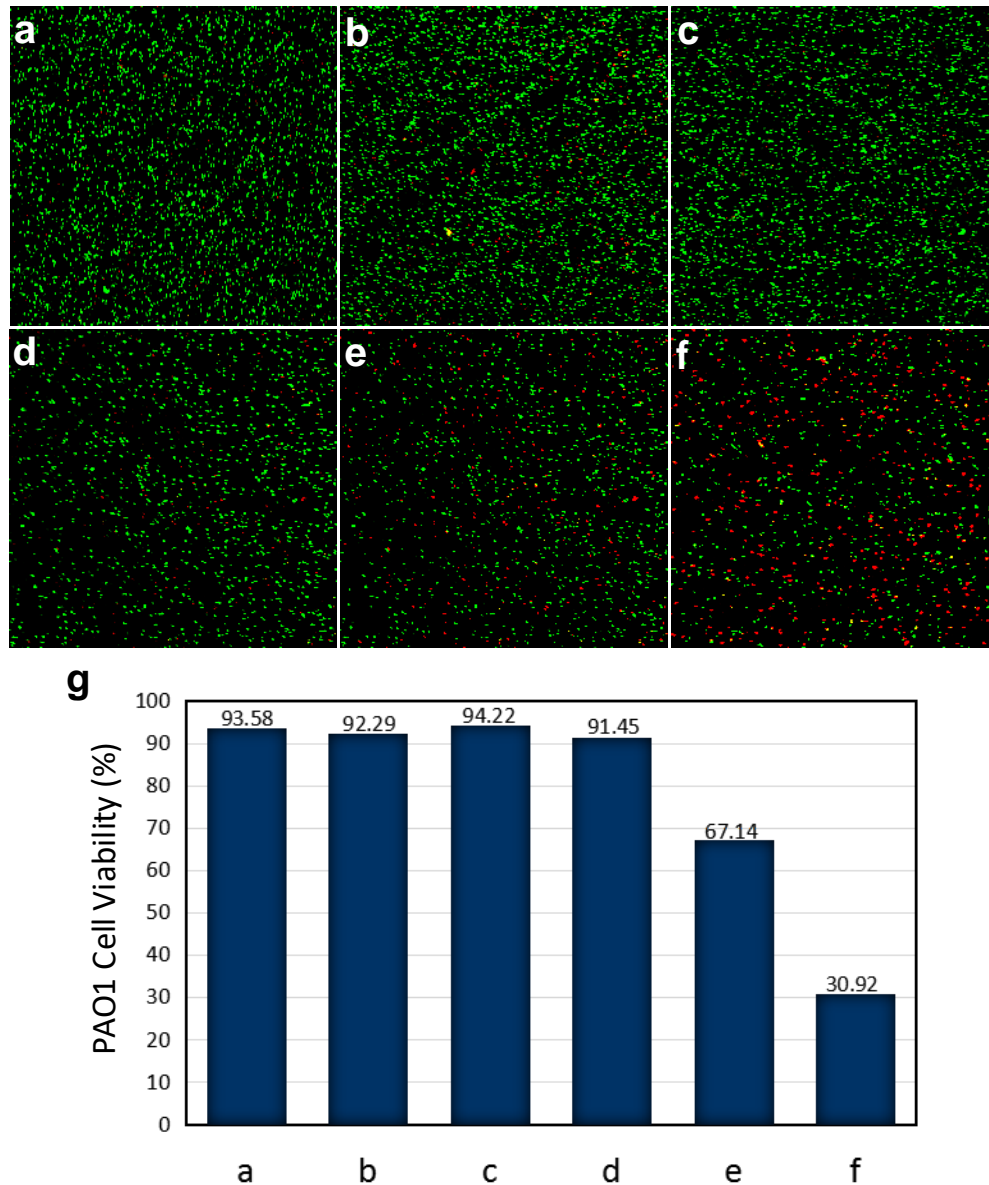
Figure 5. | Confocal microscopy of PAO1 cells showing lysosomes stained by Syto9 and propidium iodide. a, Group1 of PAO1 irradiated by X-ray. **b**, Group2 of PAO1 with β-NaYF$_4$: Tb^{3+} irradiated by X-ray. **c**, Group3 of PAO1 with g-C$_3$N$_4$. **d**, Group4 of PAO1 with g-C$_3$N$_4$ irradiated by X-ray. **e**, Group5 of PAO1 with β-NaYF$_4$: Tb^{3+} and g-C$_3$N$_4$ irradiated by X-ray but took the β-NaYF$_4$: Tb^{3+} away immediately after ceasing the X-ray irradiation. **f**, Group6 of PAO1 with β-NaYF$_4$: Tb^{3+} and g-C$_3$N$_4$ irradiated by X-ray. X-ray Exposures: upon 30 mA, 50 kVp for 2 min. Images of all groups were obtained after being placed in a darkroom for 5 h. **g**, Comparison of PAO1 cells viability in six groups.